ISSN 0021-3640, JETP Letters, 2013, Vol. 97, No. 1, pp. 20–27. © Pleiades Publishing, Inc., 2013.
Original Russian Text © Yu.V. Petrov, N.A. Inogamov, K.P. Migdal, 2013, published in Pis'ma v Zhurnal Eksperimental'noi i Teoreticheskoi Fiziki, 2013, Vol. 97, No. 1, pp. 24–31.

Thermal Conductivity and the Electron–Ion Heat Transfer Coefficient in Condensed Media with a Strongly Excited Electron Subsystem

Yu. V. Petrov[a], N. A. Inogamov[a, *], and K. P. Migdal[b]

[a] *Landau Institute for Theoretical Physics, Russian Academy of Sciences, Chernogolovka, Moscow region, 142432 Russia*

* *e-mail: nailinogamov@googlemail.com*

[b] *All-Russia Research Institute of Automatics, Moscow, 127055 Russia*

Received November 15, 2012

The two-temperature ($T_e > T_i$) thermal conductivity coefficient κ_{2T} and electron–ion heat transfer coefficient α, which are necessary for the quantitative description of the processes initiated by ultrashort laser pulse, have been calculated using a kinetic equation, the matrix element for the scattering probability, and a screened Coulomb potential describing the interaction between charged particles. Quantitative information has been obtained for coefficients κ_{2T} and α values for noble and transition metals, where the *d*-band electrons play a significant role.

DOI: 10.1134/S0021364013010098

An ultrashort laser pulse incident on a solid target creates a two-temperature ($2T$) medium ($T_e \gg T_i$) with a solid-state density [1–4]. The difference of the electron temperature T_e from T_i is due to the fact that the duration of the ultrashort laser pulse τ_L is shorter the electron–ion relaxation time t_{eq} in which the temperatures T_e and T_i become equal to each other [1, 5–7]. At absorbed energies F_{abs} about and above the thermomechanical ablation threshold ($F_{abs}|_{abl} \sim 100$ mJ/cm^2) [8–11], the number of electrons excited above the Fermi level is large, the electron–electron (e–e) collision frequency ν_{ee} is high, e–e thermalization occurs rapidly, and the Fermi function $f(\varepsilon;\ T_e,\ \mu) = [1 + e^{(\varepsilon-\mu)/k_B T_e}]^{-1}$ with the chemical potential $\mu(T_e)$ can be used as the electron distribution function even at times $\tau_L \sim 10$–100 fs. The calculations reported in [12] indicate that the thermodynamic description of the electron subsystem is applicable when the energies $F_{abs}|_{abl}$ are higher than ~1 mJ/cm^2 ~ 1% of the threshold $F_{abs}|_{abl}$.

1. ROLES OF *s* AND *d* ELECTRONS

New data on the $2T$ thermal conductivity $\kappa_{2T} = \kappa(T_i,\ T_e)$ and the electron–ion heat transfer coefficient α of noble and transition *d* metals Au, Ni, Fe, and Ta are obtained and compared with the previously calculated functions κ_{2T} [13] and α [2, 4]. The calculations in [2, 4, 13] were performed within a similar method, but only for a simple case of a single-band metal (e.g., Al). In addition, our results are compared to the data on α for *d* metals from [3]. The approach used in this work significantly differs from the approach that was used in [3, 14]. The approach [3, 14] is based on the simplifying assumption of the equality of the matrix elements for the *s* and *d* bands [14].

We assume that the electron subsystem consists of *s* and *d* electrons (in this case, *s* electrons are the generalized name for *s* and *p* electrons if the latter exist, e.g., for the case Al $3s^2 3p^1$). The electron spectrum is approximated by parabolas for *s* and *d* electrons:

$$g_s = \frac{\sqrt{2}}{\pi^2}\frac{m_s^{3/2}}{n_{at}\hbar^3}\sqrt{\varepsilon - \varepsilon_s}, \quad m_s = \frac{(3\pi^2)^{2/3}}{2}\frac{\hbar^2 n_s^{2/3}}{\mu_0 - e_s}. \quad (1)$$

Here, n_{at} and n_s are the atomic and *s* electron densities, respectively, and $\mu_0 \equiv \mu(0)$ is the chemical potential $\mu(T_e)$ at zero temperature. The expressions for the electron density of states g_d per atom and for the effective mass m_d of *d* electrons are similar to Eqs. (1). The electron dispersion relations have the form

$$\varepsilon(\mathbf{p}) = \varepsilon_s + p^2/2m_s, \quad \varepsilon(\mathbf{p}') = \varepsilon_1 + p'^2/2m_d. \quad (2)$$

The parameters entering into Eqs. (1) and (2) are presented in the table and their meaning is illustrated in Fig. 1. The energies ε_s, ε_1, and ε_2 are measured from $\mu(0)$. The quantities $Z_s(T_e) = n_s(T_e)/n_{at}$ and $Z_d(T_e)$ at zero temperature are $Z_s(0) = 3$ and $Z_d(0) = 0$ for Al, $Z_s(0) = 1$ and $Z_d(0) = 10$ for Au, $Z_s(0) = 1.5$ and $Z_d(0) = 8.5$ for Ni, $Z_s(0) = 2$ and $Z_d(0) = 6$ for Fe, and

$Z_s(0) = 2$ and $Z_d(0) = 3$ for Ta. The masses m_s and m_d are normalized to the mass of the free electron.

Figure 1 shows the electronic spectrum of nickel and its two-parabolic approximation by Eqs. (1) and (2). The spectrum was calculated within the density functional theory using the DMol^3 code [15] taking into account all 28 electrons of Ni. The electronic spectra of Al, Au, Fe, and Ta were calculated using the ABINIT DFT packet [16], which requires a pseudopotential [17]. The d band for Au, Ni, Fe, and Ta is much narrower than the s band. Correspondingly, d electrons are heavier. The ε_2 point is the upper edge of the d band. This edge for noble metals is below the μ_0 level. The ε_2 point for transition metals is above the μ_0 level. This edge is particularly close to μ_0 in Ni.

We assume that s and d electrons are in thermodynamic equilibrium between each other and, therefore, constitute a united thermodynamic subsystem with a common chemical potential. Indeed, the huge ion-to-electron mass ratio, which is responsible for the two-temperature regime, is much larger than the ratio m_d/m_s. Correspondingly, the three-temperature situation is absent.

Electrons of the s band are more mobile. For this reason, charge and heat transport occurs primarily through s electrons.

2. SUMMATION OF ELECTRON–ION AND ELECTRON–ELECTRON COLLISION FREQUENCIES

We use the effective frequencies determined by the Drude formulas

$$\sigma = \frac{n_s(T_e)e^2}{m_s(\nu_{si} + \nu_{sd})}, \quad \kappa = \frac{1}{3}\frac{C_s(T_e)\bar{v}_s^2(T_e)}{\nu_{si} + \nu_{se}}. \qquad (3)$$

Here, the subscript si refers to the collisions of s electrons with ions. The specific heat C_s and average square $\bar{v}_s^2$ of the velocity of s electrons are calculated within the two-parabolic spectral model presented in Fig. 1. The frequency $\nu_{se} = \nu_{ss} + \nu_{sd}$ is the sum of the scattering frequencies of s electrons from each other and from d electrons. The electric resistivity has no contribution from s–s collisions because umklapp effects are insignificant. For this reason, the denominators in Eqs. (3) for σ and κ contain the sums $\nu_{si} + \nu_{sd}$ and $\nu_{si} + \nu_{ss} + \nu_{sd}$, respectively.

The effective frequencies determined from Eqs. (3) play an auxiliary role and do not appear in the final expressions for the $2T$ thermal conductivity $\kappa_{2T} = \kappa(T_i, T_e)$. The thermal resistivity $1/\kappa_{2T}$ is the sum $1/\kappa_{2T} = 1/\kappa_{si} + 1/\kappa_{se}$ of the resistivities associated with s–i and s–e scattering events, respectively (Mattissen rule). The partial thermal conductivities κ_{si} and κ_{se} are reliably determined from existing experimental data

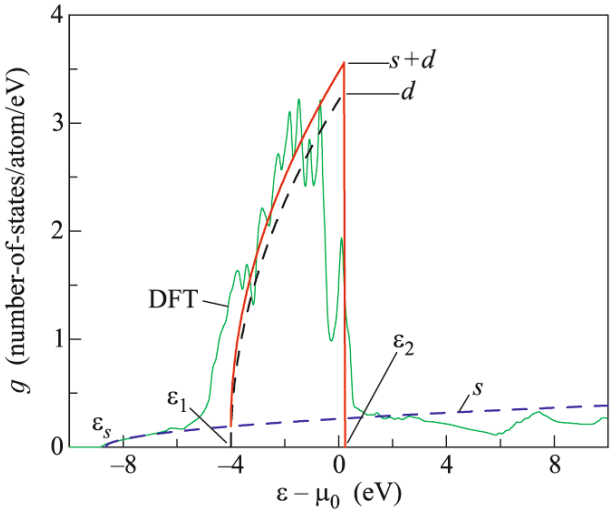

Fig. 1. Approximate description of the band structure of nickel with the s and d parabolas.

(Section 3) and from the kinetic equation in the τ approximation (Section 4), respectively.

3. ELECTRON–ION CONTRIBUTION TO THE RESISTIVITY

Electron–electron processes dominate in the resistivity of d metals only at low (much lower than the Debye temperature θ) and high (about several electronvolts) temperatures. Phonons are frozen at low temperatures (see [13] and references therein). The $2T$ situation, where electrons are hot ($T_e > 1$ eV) and T_i values are moderate, is implemented at high temperatures. Our calculations were performed for the T_i range from θ to the temperature T_* several times higher than the melting temperature T_m.

In the one-temperature (κ_{1T}) case ($T_e = T_i = T$), i.e., in the range $\theta < T < T_*$, the coefficient $\kappa_{1T} = \kappa(T)$ is determined by the electron–ion interaction (the contribution from e–e processes is insignificant) and is studied in detail both experimentally and theoretically. The corresponding dependences are summarized in the standard handbooks on physical quantities. Theoretical calculations of the κ_{1T} conductivity are based on the kinetic equation and screened Coulomb inter-

Parameters describing the spectrum

	ε_s, eV	ε_1	ε_2	m_s/m	m_d/m
Al	–11.1			1.05	
Au	–9.2	–6.8	–1.7	0.6	5.4
Ni	–8.6	–4.5	0.17	1.1	6.9
Fe	–8.7	–4.9	1.4	1.3	4.8
Ta	–8	–4.6	5.9	1.1	2.4

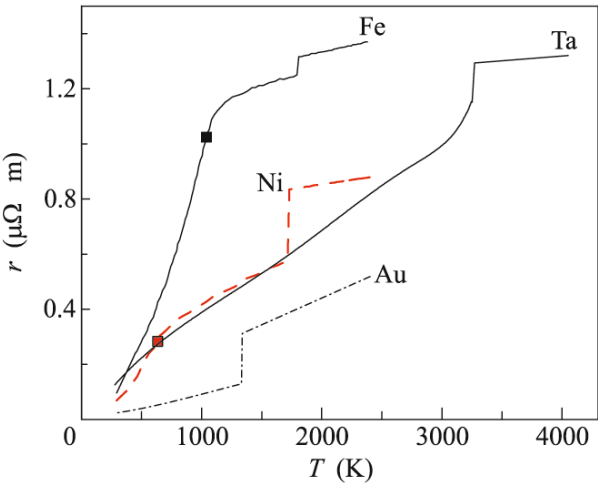

Fig. 2. Temperature dependences of the resistivity $r(T)$; the resistivity r increases continuously with the temperature and stepwise upon melting.

action. Such calculations are in good agreement with the measurements. Such a theoretical approach is applied in Sections 4 and 5 to calculate the coefficients κ_{2T} and α in the $2T$ situation.

It is noteworthy that κ_{ee} was recently calculated in [13] taking into account only s–s scattering. Using the results reported in [13], Gill-Comeau and Lewis [18] obtained the ablation threshold $F_{\text{abs}}|_{\text{abl}} = (60–80)$ mJ/cm^2 for Al in agreement with our results [19–21]. Various approaches to the calculation of κ_{2T} were compared in [22]. The case of Al $3s^2 3p$, which is a $2T$ metal with one band, was considered in [13]. Sections 4 and 5 present new results generalizing the approach with the kinetic equation to a complex two-band case with s–d scattering. This case is important for d metals.

Figure 2 shows the temperature dependences of the $1T$ resistivity that were obtained from the modern measurements of the resistance of thin wires heated by a current pulse (see, e.g., [23]). Such experiments provide measurements at temperatures significantly higher than the melting temperature. The resistivity r in the solid phase of pure metals above the Debye temperature is proportional to T because of an increase both in the amplitude of thermal vibrations of ions in a lattice and in the cross section for electron–phonon interaction. The linear behavior in metals with magnetic properties (Ni, Fe, see Fig. 2) continues up to the Curie point (marked by a square). The linear temperature dependence for iron reaches a large value of about 1 μΩ m. This value is comparable with the maximum metallic resistivity $r_{\max} \sim m_e v_F/n_s e^2 a \sim \hbar/e^2 a \sim 1$ μΩ m (the maximum value v_F/a, where v_F is the Fermi velocity and a is the lattice constant, is taken for the collision frequency ν).

The $r(T)$ dependence in transition metals above the Curie temperature or the melting temperature cannot be approximated by the expression $r \approx a + bT$ with a small constant a. The constant a is no longer small and the slope dr/dT decreases significantly (see Fig. 2). This behavior indicates that an increase in $r(T)$ is saturated owing to approaching the limit $r_{\max}$. The resistivity r in the solid phase in our model is approximated according to the experimental data shown in Fig. 2, whereas the formula $r = (r_{\text{lin}}^{-2} + r_{\max}^{-2})^{-1/2}$ is used for a melt. This formula matches the linear approximation $r_{\text{lin}} = a + bT$ of the experimental data for a fluid with the limit $r_{\max}$. Then, the frequency ν_{si} is determined from the expression for σ in Eqs. (3).

The choice $r_{\max} \sim (2–5)$ μΩ m weakly affects the value $\nu_{si}(T)$ in the temperature range up to 10 kK under investigation. The resulting function $\nu_{si}(T)$ in the $2T$ situation is represented as $\nu_{si}(T_i)$; i.e., it is assumed that scattering from heavy particles at a fixed density depends primarily on the degree of ordering of the ion subsystem. This assumption was also accepted in the preceding approaches, but the authors used only the linear approximation of the function $r(T)$ and disregarded both the existence of the Curie point and a change in the coefficients of the linear function $r(T)$ upon melting.

The ablation threshold $F_{\text{abs}}|_{\text{abl}}$ is higher than the melting threshold by a factor of 2–4. Thermal loads of about the ablation threshold or higher are studied in this work. In this case, melting occurs in the $2T$ relaxation time range, because the temperature of the ion subsystem even in this range is above the temperature on the crystal–melt transition spinodal [5]. The κ_{2T} value changes after melting. This change affects the propagation of the absorbed heat F_{abs} into the bulk of the metal at the $2T$ stage and, therefore, affects the thickness d_T of the laser-heated layer.

4. ELECTRON–ELECTRON s–s AND s–d INTERACTIONS

We consider the scattering of s and d electrons satisfying dispersion relations (2). The s–s collisions were considered in [13]. The effective frequency ν_{sd} in the sum $\nu_{se} = \nu_{ss} + \nu_{sd}$ was calculated as follows. First, we calculated the time $\tau_{sd}(\mathbf{p}) = 1/\nu_{sd}(\mathbf{p})$ for an s electron with the momentum $\mathbf{p}$. This time enters into the kinetic equation in the τ approximation. The thermal conductivity coefficient κ_{sd} and electric conductivity coefficient σ_{sd} were determined from the kinetic equation. Then, the effective frequency ν_{sd} was obtained from Eqs. (3) either for the coefficient κ_{sd} or for the coefficient σ_{sd}.

The calculation stages associated with the solution of the kinetic equation and Eqs. (3) are similar for the respective calculation stages for the effective frequency ν_{ss} [13]. The stage of the calculation of the function $\nu_{sd}(\mathbf{p})$ is the most difficult. It qualitatively dif-

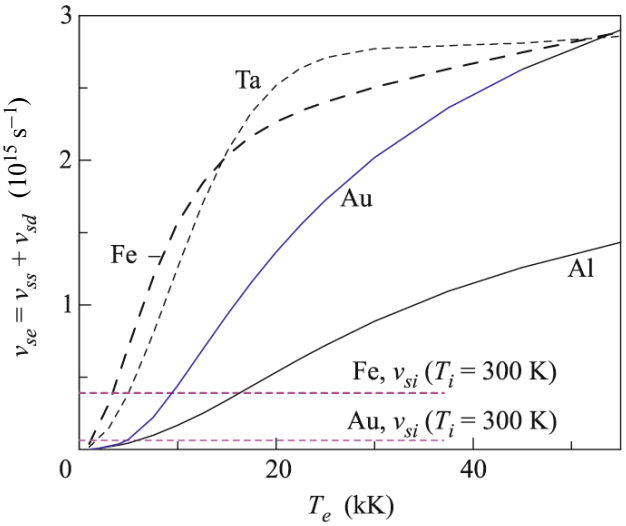

Fig. 3. Effective frequencies ν_{se} for simple, noble, and transition metals. For Al, $\nu_{se} = \nu_{ss}$. The electron–electron frequency in *d* metals is much higher than that in Al. The frequency ν_{se} in transition metals (Ni, Fe, Ta) is higher at moderate temperatures $T_e < 1$ eV owing to the contribution from *s*–*d* collisions whose frequency at these temperatures is higher than ν_{ss}. The temperature dependence of the frequency ν_{se} for Ni is not shown, because it is similar to the dependence for Fe. The horizontal straight lines are the frequencies ν_{si} at $T_i = 300$ K.

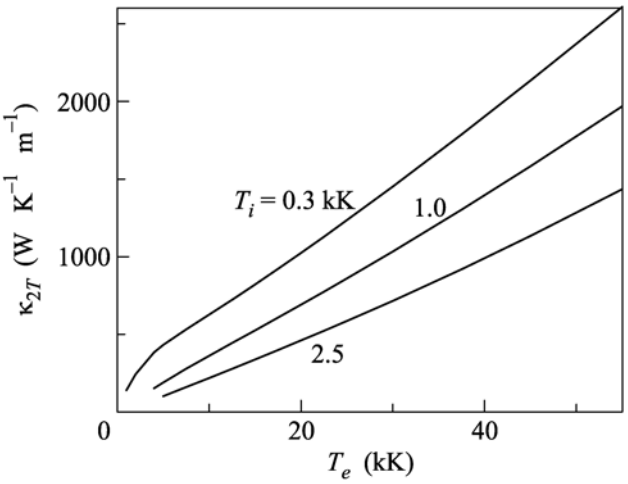

Fig. 4. Temperature dependences of the $2T$ thermal conductivity coefficient for nickel. The ion temperature is shown near the lines. It can be seen that the coefficient κ_{2T} can be much larger the reference value $\kappa_{1T} = 91$ W K^{-1} m^{-1} at room temperature.

fers from the calculation of the function $\nu_{ss}(\mathbf{p})$ in [13], because it is necessary to calculate a multiple integral including statistical factor for electrons from different bands (see Fig. 1). This circumstance strongly complicates the calculations, because the *d* band has the upper limit ε_2, which is absent for the *s* band.

The collision frequency $\nu_{sd}(\mathbf{p})$ between an *s* electron with the momentum *p* and *d* electrons is given by the formula

$$\nu_{sd}(\mathbf{p}) = \frac{2\pi}{\hbar}\int\frac{u^2(q)d^3q}{(2\pi\hbar)^3}\int\frac{2d^3p'}{(2\pi\hbar)^3}S\delta. \qquad (4)$$

This formula is written for the collision $\mathbf{p} + \mathbf{p}' \longrightarrow (\mathbf{p} + \mathbf{q}) + (\mathbf{p}' - \mathbf{q})$ between the *s* electron with the momentum $\mathbf{p}$ and a *d* electron with the momentum $\mathbf{p}'$, where *q* is the momentum transfer. The function

$$\delta = \delta[\varepsilon(\mathbf{p}) + \varepsilon'(\mathbf{p}') - \varepsilon(\mathbf{p} + \mathbf{q}) - \varepsilon'(\mathbf{p}' - \mathbf{q})]$$

ensures the energy conservation law in Eq. (4). The statistical factor *S* in Eq. (4) has the form

$$S(\mathbf{p}, \mathbf{p}', \mathbf{q}) = f_d(\mathbf{p}')[1 - f_s(\mathbf{p} + \mathbf{q})][1 - f_d(\mathbf{p}' - \mathbf{q})]$$
$$+ f_s(\mathbf{p} + \mathbf{q})f_d(\mathbf{p}' - \mathbf{q})[1 - f_d(\mathbf{p}')],$$

where f_s and f_d are the Fermi distributions for *s* and *d* electrons, respectively. In Eq. (4), $u(q)$ is the Fourier transform of the screened Coulomb interaction $u(r) = e^2\exp(-r/\lambda)/r$, where λ is the Lindhard screening length [24, 25].

Formula (4) is used to calculate (using the kinetic equation) the thermal conductivity coefficient $\kappa_{sd}(T_e)$ associated with *s*–*d* scattering. The solution of the kinetic equation has the form

$$\kappa_{sd} = \int(\varepsilon - \mu)(-f_s')\left(\mu' + \frac{\varepsilon - \mu}{T_e}\right)\frac{\overline{v_s^2}(p)}{\nu_{sd}(p)}\frac{p^2dp}{3\pi^2\hbar^3}, \qquad (5)$$

where $f_s' = \partial f_s(\varepsilon)/\partial\varepsilon$, $\mu' = \partial\mu/\partial T_e$, and v_s is the velocity of *s* electrons. A number of changes and intermediate analytical integration reduce sixfold integral (4) to a double integral over the plane ($q = |\mathbf{q}|$, $p' = |\mathbf{p}'|$). This double integral $\nu_{sd}(\mathbf{p})$ is substituted into Eq. (5); then, the resulting triple integral is numerically integrated using the Mathematica symbolic software program.

The effective frequencies $\nu_{sd} = C_s\overline{v_s^2}/3\kappa_{sd}$ and $\nu_{ss} = C_s\overline{v_s^2}/3\kappa_{ss}$ are determined from Eqs. (5) and (3) under the assumption that the electronic spectra at a fixed matter density depend only slightly on the ion temperature T_i. The dependences $\nu_{se}(T_e) = \nu_{ss} + \nu_{sd}$ calculated for the first time for noble and transition *d* metals are shown in Fig. 3.

Figure 4 shows the coefficient $\kappa(T_e, T_i)$ finally obtained taking into account *s*–*i* (see Section 3), *s*–*s*, and *s*–*d* processes. The *s*–*e* contribution to κ_{2T} in the T_e range shown in the figure is larger than the *s*–*i* contribution only for temperatures T_i below ~1 kK. Figure 5 shows the coefficient κ_{2T} for various metals. It can be seen that the thermal conductivity of Ta and Fe is much smaller than the thermal conductivity of Al and Au. Correspondingly, the heated layer in Ta and Fe

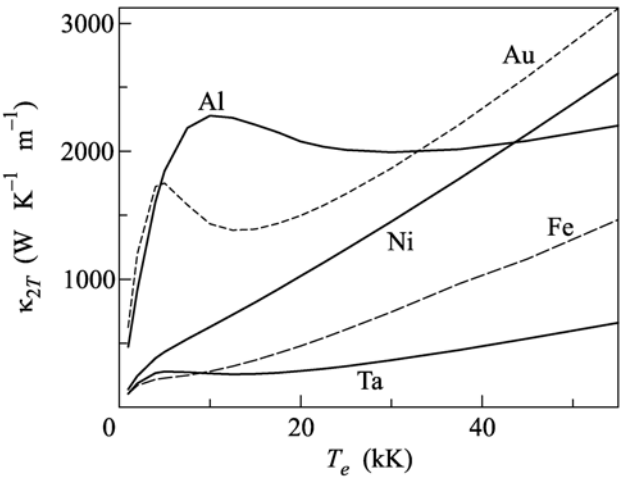

Fig. 5. Temperature dependences of the thermal conductivity $\kappa(T_e, T_i = 300\ \text{K})$ for simple, noble, and transition metals.

is narrower. According to Figs. 4 and 5, the linear dependence

$$\kappa \approx \kappa_{1T}(T = 300\ \text{K})\, T_e/T_i \tag{6}$$

is saturated at $T_e \sim 2$–5 kK owing to s–e collisions. Formula (6) is valid if the temperature dependence of κ_{1T} is weak. This formula is applicable under the condition $\nu_{se} < \nu_{si}$, i.e., when scattering from heavy particles dominates. The behavior $\kappa(T_e, T_i)$ for noble metals is interesting. Figure 5 demonstrates the existence of a quite narrow maximum and a decrease in κ with an increase in T_e in a certain temperature range in the case of gold. A decrease in the coefficient κ_{2T} with an increase in the temperature T_e was possibly detected in the recent experiment with gold [26].

5. HEAT TRANSFER RATE FROM HOT ELECTRONS TO THE ION SUBSYSTEM

According to classical work by Kaganov, Lifshitz, and Tanatarov [27], the energy transferred from electrons to ions in unit time and unit volume at $T_e > T_i$ is given by the expression

$$\dot{E} = \int \hbar\omega_{\mathbf{q}} \dot{N}_{\mathbf{q}} V d\mathbf{q}/(2\pi\hbar)^3 = \alpha(T_e)(T_e - T_i). \tag{7}$$

This formula is written in terms of the volume of the system V rather than unit volume. In this representation, it is clear that the number of cells $Vd\mathbf{q}/(2\pi\hbar)^3$ is dimensionless. The quantity $\dot{N}_{\mathbf{q}}$ and probability $W_{\mathbf{q}}$ will be defined below. The electron–phonon heat transfer coefficient is independent of the temperature T_i if $T_i \gg \theta$. The formulas below can be generalized to the case $T_i \sim \theta$. In this case, the coefficient α changes slightly as compared to that calculated under the assumption that $T_i \gg \theta$.

Heat flux (7) is due to the Cherenkov emission of phonons by supersonic electrons and is nonzero if the temperatures of the thermodynamically equilibrium electron and ion subsystems are different. The quantity

$$\dot{N}_{\mathbf{q}} = 2\int \Phi W_{\mathbf{q}} \delta(\varepsilon_{\mathbf{p}-\mathbf{q}} + \hbar\omega_{\mathbf{q}} - \varepsilon_{\mathbf{p}}) d\mathbf{p}/(2\pi\hbar)^3$$

in Eq. (7) is the rate of change in the number density of longitudinal phonons $N_{\mathbf{q}}(t)$ with the momentum $\mathbf{q}$ and energy $\hbar\omega_{\mathbf{q}}$ owing to the spontaneous and induced emission of phonons. Here and below,

$$\Phi = (1 - f_{\mathbf{p}-\mathbf{q}}) f_{\mathbf{p}} + N(\mathbf{q})[(1 - f_{\mathbf{p}-\mathbf{q}}) f_{\mathbf{p}} - (1 - f_{\mathbf{p}}) f_{\mathbf{p}-\mathbf{q}}]$$

is the statistical factor involving the Fermi distribution $f(\varepsilon;\ T_e,\ \mu)$ for electrons and the Bose distribution $N(q) = (e^{\hbar\omega_{\mathbf{q}}/k_{\mathrm{B}}T_i} - 1)^{-1}$ for phonons. The phonon dispersion relation $\omega_{\mathbf{q}} = c_s|\mathbf{q}|/\hbar$ is written in the Debye approximation.

The probability of the transition of an electron from a state with the momentum $\mathbf{p}$ to a state with the momentum $\mathbf{p} - \mathbf{q}$ in unit time is $W_{\mathbf{q}}\delta(\varepsilon_{\mathbf{p}-\mathbf{q}} + \hbar\omega_{\mathbf{q}} - \varepsilon_{\mathbf{p}})$. Electrons in metals interact with longitudinal acoustic phonons. In this case, this probability is given by the expression

$$\begin{aligned} W_{\mathbf{q}} &= \pi\omega_{\mathbf{q}} U^2(\mathbf{q})/\rho V c_s^2, \\ U(\mathbf{q}) &= 4\pi e^2\hbar^2 Z_i n_{\mathrm{at}}/q^2\epsilon(\mathbf{q}), \end{aligned} \tag{8}$$

where $U(\mathbf{q})$ is the Fourier transform of the screened Coulomb potential; $\epsilon(\mathbf{q})$ is the dielectric constant, which is calculated in the Lindhard approximation [24, 25] similar to the calculations of s–s and s–d collisions in Section 4; Z_i is the effective charge number of the ion; and n_{at} is the number density of atoms. In Eq. (7), $\alpha = \alpha_s + \alpha_d$. The coefficients α_s and α_d are calculated individually. In the case of the coefficient α_s, Z_i in Eq. (8) is $Z_s = n_s(T_e)/n_{\mathrm{at}}$. In the case of the coefficient α_d, $Z_i = Z_s(T_e) + Z_d(T_e) = \text{const}$, because the ionization of electron shells below the s and d bands can be neglected at the temperatures T_e of interest. In particular, $Z_s + Z_d = 10$ for nickel (see the fourth sentence after Eq. (2)).

The formula for the coefficient α can be simplified after cumbersome calculations. For heat transfer from the d band to the lattice, the expression has the form

$$\alpha_d = \frac{m_d^2}{4\pi^3\hbar^7}\frac{k_{\mathrm{B}}^2 T_e}{\rho c_s}\int_0^{q_{\mathrm{D}}} dq q^2 U^2(\mathbf{q}) \ln\frac{e_1 + e_2}{e_1 + 1}\bigg|_{\varepsilon = a}^{\varepsilon = b}, \tag{9}$$

where

$$e_1 = \exp\frac{\varepsilon - \mu - \hbar\omega_q}{k_{\mathrm{B}}T_e}, \quad e_2 = \exp\left(-\frac{\hbar\omega_q}{k_{\mathrm{B}}T_e}\right),$$

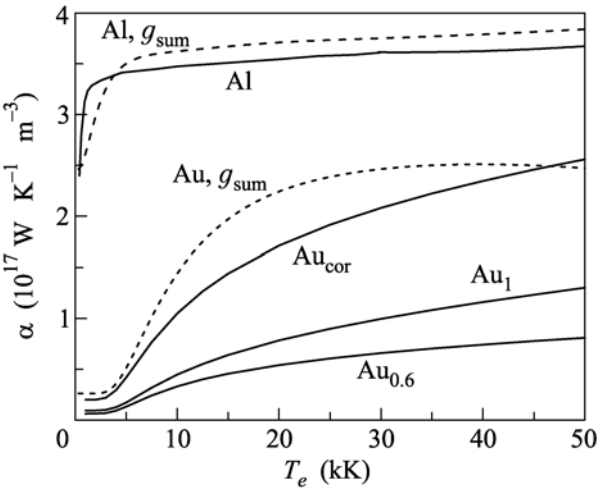

Fig. 6. Dependences $\alpha(T_e)$ calculated in this work in comparison with those taken from [3], which are marked by g_{sum}, meaning that α was calculated by Eq. (11) in terms of the total electron density of states.

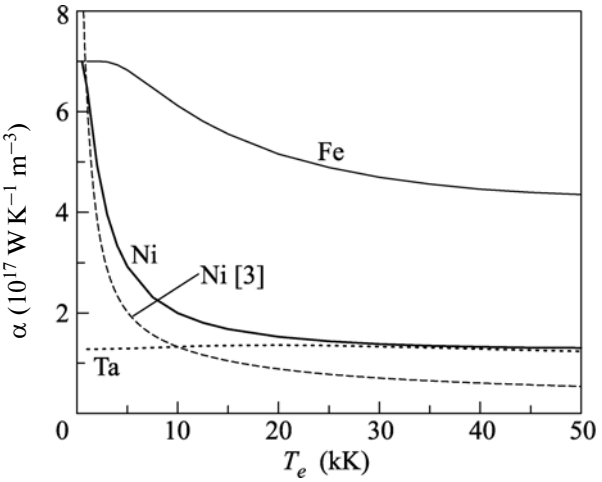

Fig. 7. Dependences $\alpha(T_e)$ calculated for nickel, iron, and tantalum using Eq. (9). The dashed line marked by Ni [3] is taken from [3].

$$a = \varepsilon_1 + \frac{1}{2m_d}\left(\frac{q}{2} + m_d c_s\right)^2, \quad b = \varepsilon_1 + \frac{p_d^2}{2m_d},$$

and q_D is the Debye momentum. The expression for α_s is simpler than Eq. (9). It is important that these expressions do not contain the ion temperature at $T_i \gg \theta$.

Figures 6 and 7 show the coefficients $\alpha = \alpha_s + \alpha_d$ obtained with Eq. (9) for α_d and the expression for α_s. We now compare our results from the previous data. The dependence of α on the temperature T_e was neglected in early calculations of the coefficient α [27, 28]. In fundamental work [27], the matrix element in the formula for α was estimated, rather than calculated. In important work [28], the connection with superconductivity was revealed and the formula for α from [27] was reduced to the expression

$$\alpha = \pi\hbar k_B \lambda \langle\omega^2\rangle g(\varepsilon_F), \qquad (10)$$

where $g(\varepsilon)$ is the electron density of states (see, e.g., Fig. 1) and ε_F is the Fermi energy. The quantities λ and $\langle\omega^2\rangle$ in Eq. (10) are related to the Eliashberg spectral function and theory of superconductivity [3, 28, 14]. Thus, the coefficient α can be determined knowing the factor $\lambda\langle\omega^2\rangle$. The $\lambda\langle\omega^2\rangle$ values for a number of metals were presented in [3, 29].

Wang et al. [14] emphasized that Eq. (10) is applicable only for fairly low temperatures T_e and its generalization was proposed. This generalization has the form

$$\alpha = \pi\hbar k_B \lambda \langle\omega^2\rangle \int d\varepsilon g^2(\varepsilon)(-\partial f/\partial\varepsilon)/g(\varepsilon_F), \qquad (11)$$

where f is the Fermi distribution. Thus, the factor $g(\varepsilon_F) = g_F$ in Eq. (10) was changed to the factor $[\int(-f')g^2]/g(\varepsilon_F)$. As a result, a significant electron-temperature dependence appears because f' is a function of T_e.

Another important feature of Eq. (11) is as follows. The *total* density of states g_{sum} is taken as the electronic spectrum in Eq. (11). In *d* metals under consideration with *s* and *d* bands, $g_{sum} = g_s + g_d$ (see Fig. 1). The significant energy dependence of the spectrum $g_{sum}(\varepsilon)$ that is characteristic of *d* metals enhances the temperature dependence $\alpha(T_e)$. The dependence on T_e for noble metals with $\varepsilon_2 < 0$ differs from that for transition metals with $\varepsilon_2 > 0$ [3]. The definition of ε_2 is given in Fig. 1 and in the table. The function $\alpha(T_e)$ increases and decreases with an increase in T_e at $\varepsilon_2 < 0$ and $\varepsilon_2 > 0$, respectively.

The approach with the total spectrum g_{sum} is empirical. In deriving this approach, the energy dependence of the matrix element in the scattering probability is neglected [3, 14]. It is even more important that the difference between the matrix elements for the *s* and *d* bands is neglected. At the same time, the characteristics of the *s* and *d* bands are strongly different (see table). The total electronic specific heat is really calculated in terms of the spectrum g_{sum}. However, the transport characteristics (σ and κ) of *s* and *d* electrons are different (see Section 4). Correspondingly, there are no reasons for the assumption of the equality of the matrix elements for the *s* and *d* bands.

Figures 6 and 7 show the results of the direct calculation of α by Eq. (9) without any assumptions concerning the matrix elements for the *s* and *d* bands. It is worth noting that Eq. (10) (relation between α and

$\lambda\langle\omega^2\rangle$) is of insignificant theoretical importance, because the factor $\lambda\langle\omega^2\rangle$ is often obtained from measurements of the coefficient α [29]. The same concerns Eq. (11), which differs from Eq. (10) only in a factor. The dependence $\alpha(T_e)$ given by Eq. (11) starts at room temperature T_e from the experimental value α_{rt}, which changes with the temperature according to the factor $-\int f' g^2/g_F^2$.

Figure 6 shows α values calculated by formulas similar to Eq. (9) in comparison to the results obtained by Eq. (11). As can be seen, agreement between calculations for single-band metal Al is good. A close value was obtained in [4]. It is noteworthy that the recent experiment [30] gives a value of 1.2×10^{17} W K^{-1} m^{-3} for the coefficient α in aluminum, which is smaller than a theoretical value of $(3–3.6) \times 10^{17}$ W K^{-1} m^{-3} by a factor of 2.5–3 and is the half of the value corresponding to the experiment reported in [31] (see discussion in [30]). It is worth noting that the function $\alpha(T_e)$ (see data for Al in Fig. 6) varies slightly with the electron temperature at a smooth single-band spectrum.

We now analyze the situation for gold as an example of noble metals. Figure 6 shows four $\alpha(T_e)$ dependences marked as Au, g_{sum}, $Au_{0.6}$, Au_1, and Au_{cor}. The Au, g_{sum} curve obtained by Eq. (11) is taken from [3]. The $Au_{0.6}$ and Au_1 curves (the subscript indicates the effective mass of the *s* electron) were obtained by Eq. (9). The parameters of the electronic spectrum of gold that were used to obtain the $Au_{0.6}$ curve were the same as in the table. For the Au_1 curve, the parameters of the two-parabolic approximation specified by Eqs. (1) and (2) were changed to $\varepsilon_s = 5.5$ eV and $m_s/m = 1$ and the other parameters remained unchanged. The accuracy of the calculation by Eq. (9) is limited by the accuracy of the description of the real electron density of states by the two-parabolic spectrum specified by Eqs. (1) and (2). The difference between the $Au_{0.6}$ and Au_1 curves in Fig. 6 estimates the error associated with the approximate representation of the spectrum.

According to Eq. (9), the $\alpha(T_e)$ dependence approaches the constant value $\alpha_{0.6}|_{(9)}(T_e = 300) \approx 0.06 \times 10^{17}$ W K^{-1} m^{-3}. According to the experiments [30–32], $\alpha_{exp}(T_e = 300) \approx 0.2 \times 10^{17}$ W K^{-1} m^{-3}. Thus, Eq. (9) with $m_s/m = 0.6$ and 1 for Au gives the $\alpha(300)$ value that is smaller than the experimental value by a factor of 3 and 2, respectively. The Au_{cor} in Fig. 6 corresponds to the $\alpha_{0.6}|_{(9)}(T_e)$ dependence multiplied by a factor of $\alpha_{exp}(300)/\alpha_{0.6}|_{(9)}(300)$. According to the figure, the calculations by Eq. (9), as well as [3, 14], indicate a significant increase in the coefficient α upon the heating of the electron subsystem of gold. The comparison of the partial coefficients α_s and α_d shows that the term corresponding to the heat transfer through α_d electrons dominates in the sum $\alpha = \alpha_s + \alpha_d$ for gold. The contribution α_s exceeds the contribution α_d only at relatively low temperatures $T_e < 5$ kK. For transition metals, the term α_d is decisive for all temperatures T_e.

We consider the situation with transition metals ($\varepsilon_2 > 0$), where the edge of the *d* band is above the Fermi level (see Fig. 1). There are three typical cases: with a small ε_2 value (Ni, see table), with an moderate ε_2 value (Fe), and with a large ε_2 value (Ta). These cases are characterized by three different behaviors of the function $\alpha(T_e)$ (see Fig. 7). At small ε_2 values (Ni), the coefficient $\alpha(T_e)$ decreases sharply at $k_B T_e > \varepsilon_2$. At moderate ε_2 values (Fe), this decrease is smooth. In the case of the *d* band broadened with respect to the Fermi level μ_0, the function $\alpha(T_e)$ in Fig. 7 is approximately constant (Ta).

The $\alpha(T_e)$ value for tantalum shown in Fig. 7 is determined using Eqs. (7)–(9). The functions $\alpha_{Ni}(T_e)$ and $\alpha_{Fe}(T_e)$ were also determined using this approach, but were then normalized so that the function $\alpha(T_e)$ at room temperature is $\alpha_{exp}|_{rt} \approx 7 \times 10^{17}$ W^{-1} m^{-3} for both nickel and iron. The $\alpha_{exp}|_{rt}$ value corresponds to the experimental data for nickel [3]. We believe that this value for iron will be approximately the same. For this normalization, the functions $\alpha_{Ni}(T_e)$ and $\alpha_{Fe}(T_e)$ calculated by Eqs. (7)–(9) should be reduced by a factor of 3 and 2, respectively.

The effect of the variation of the parameters of the band structure on the function $\alpha_{Ni}(T_e)$ was studied. The function $\alpha_{Ni}(T_e)$ plotted in Fig. 7 was calculated with the boundaries of the bands indicated in the table, but for $Z_s(0) = 0.6$ [33] rather than 1.5 from the table. Correspondingly, the masses change as $Z_s(0) = 0.6$, $m_s/m = 0.6$, and $m_d/m = 7.3$. The calculations by Eqs. (7)–(9) are stable with respect to variation of the parameters of the approximation given by Eqs. (1) and (2) near the real spectrum. The function $\alpha_{Ni}(T_e)$plotted in Fig. 7 has a flat section at $T_e > 10$ kK. The coefficient $\alpha_{Ni}|_{Z_s = 1.5}(T_e)$ in the flat section at $Z_s(0) = 1.5$ is larger than $\alpha_{Ni}|_{Z_s = 0.6}(T_e)$ by a factor of 1.5–2. These two functions at $T_e < 10$ kK differ only slightly. At heat inputs of about the ablation threshold $F_{abs}|_{abl} \sim 0.1$ J/cm^2, the heat transfer from the electron subsystem of nickel to ions becomes insignificant in the energy balance at $T_e < 3–5$ kK, because electrons at relatively low temperatures have low energy. For this reason, the large α values at low temperatures T_e are insignificant at these F_{abs} values.

In summary, the coefficients κ_{2T} and α necessary for the predictive numerical simulation of the process and sequences of laser action have been calculated. Existing information on metal melts has been used to calculate the electron–ion frequencies entering into

κ_{2T}. The direct calculations by Eqs. (5) and (7)–(9) provide new data on s–d scattering and coefficient α for d metals. The detailed calculation results are presented in a digital format at the website of the Landau Institute for Theoretical Physics, Russian Academy of Sciences [34].

We are grateful to V.V. Zhakhovskii and B.J. Demaske for assistance in the computer DFT calculations with the DMol^3 code (Fig. 1). This work was supported by the Russian Foundation for Basic Research (project no. 11-08-01116-a).

REFERENCES

1. S. I. Anisimov, B. L. Kapeliovich, and T. L. Perel'man, Sov. Phys. JETP **39**, 375 (1974).
2. Yu. V. Petrov, Laser Part. Beams **23**, 283 (2005).
3. Zh. Lin, L. V. Zhigilei, and V. Celli, Phys. Rev. B **77**, 075133 (2008).
4. B. Rethfeld, A. Kaiser, M. Vicanek, and G. Simon, Phys. Rev. B **65**, 214303 (2002).
5. N. A. Inogamov, V. V. Zhakhovskii, S. I. Ashitkov, et al., Appl. Surf. Sci. **255**, 9712 (2009); arXiv:0812.2965.
6. S. G. Bezhanov, A. P. Kanavin, and S. A. Uryupin, Quantum Electron. **41**, 447 (2011).
7. P. A. Loboda, N. A. Smirnov, A. A. Shadrin, et al., High Energy Density Phys. **7**, 361 (2011).
8. V. V. Zhakhovskii, K. Nishikhara, S. I. Anisimov, and N. A. Inogamov, JETP Lett. **71**, 167 (2000).
9. L. V. Zhigilei, Zh. Lin, D. S. Ivanov, et al., J. Phys. Chem. C **113**, 11892 (2009).
10. S. I. Anisimov, V. V. Zhakhovskii, N. A. Inogamov, et al., JETP Lett. **77**, 606 (2003).
11. A. Volkov and L. Zhigilei, J. Phys.: Conf. Ser. **59**, 640 (2007).
12. B. Y. Mueller, I. Klett, and B. Rethfeld, AIP Conf. Proc. **1464**, 609 (2012); doi: 10.1063/1.4739913.
13. N. Inogamov and Yu. Petrov, J. Exp. Theor. Phys. **110**, 446 (2010).
14. X. Y. Wang, D. M. Riffe, Y.-S. Lee, et al., Phys. Rev. B **50**, 8016 (1994).
15. http://accelrys.com/.
16. http://www.abinit.org.
17. http://www.abinit.org/downloads/psp-links/psp-links/gga-fhi.
18. M. Gill-Comeau and L. Lewis, Phys. Rev. B **84**, 224110 (2011).
19. V. Zhakhovskii, N. A. Inogamov, Yu. V. Petrov, et al., Appl. Surf. Sci. **255**, 9592 (2009).
20. S. I. Anisimov, N. A. Inogamov, Yu. V. Petrov, et al., Appl. Phys. A **92**, 797 (2008).
21. S. I. Anisimov, N. A. Inogamov, Yu. V. Petrov, et al., Appl. Phys. A **92**, 939 (2008).
22. M. E. Povarnitsyn, N. E. Andreev, E. M. Apfelbaum, et al., Appl. Surf. Sci. (2011). doi:10.1016/j.apsusc.2011.07.017.
23. G. Pottlacher, *High Temperature Thermophysical Properties of 22 Pure Metals* (Keiper, 2010).
24. J. Ziman, *Principles of the Theory of Solids* (Cambridge Univ., Cambridge, 1976; Mir, Moscow, 1974).
25. W. A. Harrison, *Solid State Theory* (McGraw-Hill, New York, 1970; Mir, Moscow, 1970).
26. Z. Chen, V. Sametoglu, Y. Y. Tsui, et al., Phys. Rev. Lett. **108**, 165001 (2012).
27. M. I. Kaganov, I. M. Lifshits, and L. V. Tanatarov, Sov. Phys. JETP **4**, 173 (1956).
28. P. B. Allen, Phys. Rev. Lett. **59**, 1460 (1987).
29. S. D. Brorson, A. Kazeroonian, J. S. Moodera, et al., Phys. Rev. Lett. **64**, 2172 (1990).
30. W. Ma, H. Wang, X. Zhang, and Wei Wang, Int. J. Thermophys. doi 10.1007/s10765-011-1063-2.
31. J. L. Hostetler, A. N. Smith, D. M. Czajkowsky, and P. M. Norris, Appl. Opt. **38**, 3614 (1999).
32. W. G. Ma et al., J. Appl. Phys. **108**, 064308 (2010).
33. N. F. Mott, Proc. Phys. Soc. **47**, 571 (1935).
34. laser.itp.ac.ru.

Translated by R. Tyapaev